A New Method for Analysis of Limit Cycle Behavior of the NASA/JPL 70-Meter Antenna Axis Servos

R. E. Hill
Ground Antennas and Facilities Engineering Section

A piecewise linear method of analyzing the effects of discontinuous nonlinearities on control system performance is described. The limit cycle oscillatory behavior of the system resulting from the nonlinearities is described in terms of a sequence of linear system transient responses. The equations are derived which relate the initial and the terminal conditions of successive transients and the boundary conditions imposed by the nonlinearities. The method leads to a convenient computation algorithm for prediction of limit cycle characteristics resulting from discontinuous nonlinearities such as friction, deadzones, and hysteresis.

I. Introduction

Recent occurrences where degradation of hydromechanical components has led to excessive limit cycle oscillations of the 70-m antenna axis servos have prompted investigations of the cause and possible methods of minimization of those oscillations. Excessive limit cycling is objectionable because it degrades antenna pointing accuracy, and is presumed to accelerate the mechanical wear degradation of actuator gears, bearings, and hydraulic motors. It is therefore important to devise methods to minimize limit cycling by alteration of the controller design, and to a limited extent, by installation of improved servovalves and hydraulic motors. Also, since it is presumed that limit cycling is aggravated by otherwise acceptable wear of mechanical devices, a more robust controller design with respect to limit cycling is desirable insofar as it would necessitate less frequent component replacements due to wear.

This article describes the initial progress in the analytic assessment of the limit cycles resulting from various nonlinearities in the system. The ultimate product of this effort will be a set of quantitative relationships between limit cycle behavior and the control system parameters. Such relationships will facilitate the selection of control parameters to provide the best overall combination of linear servo and limit cycle performance.

The major nonlinearities in the axis servos result from friction associated with the hydraulic motors and gear reducers comprising the control actuators, as well as deadzone and

hysteresis effects in the associated hydraulic servovalves. Four such actuators are employed in each axis to apply control torque directly to antenna-mounted bull gears [1]. Because the gear reducers are heavily preloaded to prevent backlash, the gear tooth and bearing friction contribute a significant part of the total friction in the system.

Simulation studies of limit cycle behavior are of limited usefulness as a design tool because they provide little insight associating parameter adjustments with performance, and because they require long simulation runs to identify stable limit cycle conditions. The large magnitude of the friction, which is roughly 25 percent of the maximum available control moment, makes the simple simulation models frequently used for friction inadequate for application to the 70-m axis servos [2]. More precise computer simulation models for friction involve considerable complexity and also necessitate smaller integration times, thus increasing computation time and making broadbased parameter studies impractical.

Conventional analytic methods such as the second method of Liapunov [3], which require continuity of the system function and of its partial derivatives, are not directly applicable because friction represents a discontinuity. Describing function analysis can be applied to simple cases such as the hydraulic valve, where the nonlinearity can be represented by a cascade function block. However, the friction associated with the antenna axes introduces a degree of complexity to the computation of the describing functions which make that method unattractive. Because friction effects appear to be the least tractable by conventional methods, the new method was developed for systems involving friction with provisions for incorporation of other nonlinearities at a later stage in the development.

The accuracy of this approach is limited by two factors. First, the form of combination of effects from various nonlinearities is not considered and linear superposition is not expected to apply. Second, an ideal continuous time-state variable controller is assumed and consideration of friction-induced estimator error and correction effects is deferred until later in the study. Despite these limitations the method should still be effective in identifying the course of design to minimize limit cycle behavior.

II. Theoretical Background

The phenomenon of friction is discussed in most elementary textbooks on mechanics. In the case of the axis servos, friction results in a torque in a direction opposite to the direction of motion, or in the absence of motion, a direction opposite to the net applied torque. In the finite-motion case, the friction torque is a constant amplitude known as the Coulomb friction. In the zero-motion case, the friction torque is equal and opposite to the applied torque until a critical level known as the static friction is exceeded. Thus, for any applied torque less than the static friction, the acceleration is zero and the system remains at rest. Because the friction torque instantaneously changes direction and amplitude at zero velocity, it is described by a discontinuous function.

In the presence of friction, a closed-loop linear system in motion behaves according to its linear equations of motion with a constant external torque corresponding to the Coulomb friction torque. When the system velocity reaches zero, the friction torque instantaneously changes direction and amplitude, according to the friction law described above. In most cases of interest here, the control torques are insufficient to instantaneously overcome the static friction so the system remains at rest for a finite period of time. At zero velocity, the static friction prevents any motion and effectively opens the rate and acceleration feedback loops. The system therefore behaves according to a set of open-loop linear equations which are formed from the closed-loop equations by deleting terms involving rate and acceleration. This open-loop transient response ends at the time the actuator torque becomes sufficient to overcome the static friction and motion commences.

The undisturbed system behavior can thus be described by a succession of linear transient responses with specific initial conditions and with an external torque disturbance corresponding to the Coulomb friction. The transients alternate between the open-loop and closed-loop responses with the initial conditions of each transient equal to the terminal conditions of the previous transient and the external torque alternating according to the direction of the velocity. Depending upon the initial conditions at the start of this sequence, the system either converges or diverges to a stable limit cycle. Alternatively, if a stable equilibrium exists, the system converges to the equilibrium point.

III. Applications

A. Limit Cycles in an Elementary PID Controller

A few basic insights can be obtained from analysis of the elementary proportional, integral, and derivative (PID) feedback controller of Fig. 1. The block diagram represents a system consisting of a pure inertia with rate, position, and integral error feedback and a linear, frequency-independent control amplifier and torque motor actuation device. For generality and convenience of analysis the torque gain and load inertia are lumped together in the rate loop gain K_3. The single external input U represents the external torque, and the three-

element output vector Y corresponds to integral error, position, and rate.

The state-space matrices for the linear closed-loop system of Fig. 1 are

$$\mathbf{A} = \begin{bmatrix} 0 & 1 & 0 \\ 0 & 0 & 1 \\ -K_1 & -K_2 & -K_3 \end{bmatrix} \qquad \mathbf{B} = \begin{bmatrix} 0 \\ 0 \\ J^{-1} \end{bmatrix}$$

$$\mathbf{C} = \begin{bmatrix} 1 & & \\ & 1 & \\ & & 1 \end{bmatrix} \qquad \mathbf{D} = \begin{bmatrix} 0 \\ 0 \\ 0 \end{bmatrix}$$

where

$$\dot{x} = \mathbf{A}x + \mathbf{B}U$$

and

$$Y = \mathbf{C}x + \mathbf{D}U$$

with U equal to the effective Coulomb friction torque in addition to any other external disturbance.

The open-loop system matrices $\mathbf{A}_0$, $\mathbf{B}_0$, $\mathbf{C}_0$, and $\mathbf{D}_0$ are formed from the closed-loop matrices above by substituting zeros for the columns of **A** and **C** that correspond to rate. The **B** and **D** matrices are unchanged from their closed-loop values. Thus

$$\mathbf{A}_0 = \begin{bmatrix} 0 & 1 & 0 \\ 0 & 0 & 0 \\ -K_1 & -K_2 & 0 \end{bmatrix} \qquad \mathbf{B}_0 = \begin{bmatrix} 0 \\ 0 \\ J^{-1} \end{bmatrix}$$

$$\mathbf{C}_0 = \begin{bmatrix} 1 & & \\ & 1 & \\ & & 0 \end{bmatrix} \qquad \mathbf{D}_0 = \begin{bmatrix} 0 \\ 0 \\ 0 \end{bmatrix}$$

The behavior of the elementary PID system can be inferred from the block diagram of Fig. 1 and the corresponding equations with the torque input adjusted according to the known characteristics of the friction. When the system is initially at rest, any finite position error produces an increasing control torque which eventually overcomes the friction, and the system begins to respond according to the closed-loop equations. The rate increases in a direction opposite to the initial position error until the control torque decreases to a level where the Coulomb friction decelerates the system toward zero rate. The closed-loop transient ends abruptly at the zero-rate point and subsequent behavior will again be governed by the open-loop equations.

The properties of the limit cycle oscillation are conveniently described by phase-plane projections of the three-dimensional state-space trajectories. For convenience of terminology, the plane corresponding to zero rate is referred to as the integral plane and the plane corresponding to zero integral is the rate plane. In the open-loop condition, the zero-rate condition defines a straight-line trajectory confined to the integral plane. The point of transition to closed-loop behavior is obtained from the equation describing the net torque acting on the inertia:

$$-K_1 x_1 - K_2 x_2 - K_3 x_3 + \frac{T_f}{J} = 0 \qquad (1)$$

where T_f assumes the algebraic sign of $(K_1 x_1 + K_2 x_2)$.

In the integral plane, Eq. (1) defines two parallel lines which bound the open-loop condition. Outside the plane, Eq. (1) defines two parallel flat surfaces which correspond to the zero-acceleration conditions. All closed-loop trajectories cross these surfaces when the control torque decreases to the friction level and deceleration begins. These crossings thus indicate the peak-rate points and should not be confused with a return to open-loop conditions.

The form of the closed-loop transient is recognized from the block diagram of Fig. 1 as a combination of a damped sinusoid and a decreasing exponential. The relative phase of the sinusoid and amplitude of the exponential are linear functions of the initial conditions and of the friction level. Because the determination of conditions at the zero-rate crossings requires solution of transcendental equations, a numerical evaluation method of analysis was pursued in preference to a generalized closed-form analytic method. The numerical processing was facilitated by the use of PC Matlab, an interactive scientific calculation program with extensive linear algebra capabilities.

Figure 2 shows the integral plane phase portraits of a family of typical transients similar in form to the closed-loop transients and satisfying the initial conditions of Eq. (1), for a case where the static and Coulomb friction levels correspond to 1.5 and 1 rad/sec^2 respectively. The actual closed-loop transients differ from those shown in that they end at the points

of zero rate which are recognized as the regions of zero slope in the integral plane. Figure 3 traces the sequencing between closed-loop and open-loop transients and shows convergence toward a stable limit cycle. Figure 4 shows the corresponding rate-plane projection. The open-loop portions of the trajectory are recognizable as constant position lines in the integral plane of Fig. 3 extending from the closed-loop terminal conditions (zero rate) to the open-loop initial condition line of Eq. (1). The general properties of this open-loop transient can be inferred from the eigenvalues of the open-loop $\mathbf{A}_0$ matrix, which in this case indicate a simple integration.

A few fundamental properties of the system behavior can be identified from Fig. 2 where the convergence of the unterminated transient toward the respective nodal points is evident. From the block diagram of Fig. 1 it is seen that the two nodal points correspond to the equilibrium condition where the control and friction torques combine to produce zero acceleration, rate, and position. The points of convergence thus satisfy the condition

$$|K_1 x_1| \leqslant \frac{T_{cf}}{J}$$

where T_{cf} is a positive constant corresponding to the Coulomb friction. It follows that any point on the straight line between the two nodal points corresponds to a stable equilibrium. Any point outside the nodal points or off their connecting line will result in finite acceleration and motion will continue until a stable equilibrium is reached.

Thus, the closed-loop initial conditions are dependent on the static friction and the nodal points are dependent on the Coulomb friction. Therefore, the initial condition lines will never intersect the stable equilibrium region unless the static and Coulomb levels are equal. Further, since Fig. 2 indicates that none of the possible trajectories cross zero rate at a zero-position condition, it follows that a finite limit cycle will always result unless the nodal points lie on the initial condition lines.

This leads to the conclusion that for any elementary PID controller with equal levels of static and Coulomb friction and in the absence of other nonlinearities, the system response will always converge to a stable equilibrium and no limit cycle will result. When the static friction exceeds the Coulomb friction level, the response from any initial condition off the line segment of stable equilibrium conditions will either converge or diverge to a stable limit cycle. A finite limit cycle condition will exist whether or not the closed-loop system response (the eigenvalues of **A**) is overdamped. Further, since the Coulomb friction increases the distance between the nodal points, its increase with a constant static-Coulomb friction differential is expected to increase the time required to transit the open-loop trajectory, thus increasing the limit cycle period.

To investigate the relationships between the control gain and limit cycle behavior, a set of 60 different combinations of gains was prepared and the properties of the resulting stable limit cycles were evaluated. To ensure that all results correspond to reasonable closed-loop stability, the gains were calculated to produce a family of left-hand plane (LHP) pole locations. The 60 combinations of pole locations included damping ratios of 50, 70.7, and 86.6 percent of critical and five magnitudes between 0.3535 and 1.414 sec^{-1} for the complex pair, along with four real pole locations between −2.83 and −8.0 sec^{-1}. The static and Coulomb friction levels were arbitrarily set at 10 and 0 rad/sec^2 respectively for all combinations of gain.

The limit cycle properties of interest here are the position amplitude, the peak rate, and limit cycle period. These properties are readily determined once the initial conditions for a stable limit cycle have been identified. For the elementary PID controller, the initial conditions for a stable cycle are readily determined by Eq. (1), so all that is required is to start with an arbitrary initial condition and observe the terminal conditions of the resulting closed-loop transient. When the initial and terminal positions are equal and opposite, a stable limit cycle has been described. A simple recursive routine was used to implement this process, where the initial condition for each trial was equated to the geometric mean magnitude of the initial and terminal positions of the previous trial. Instability associated with small values was avoided by substituting the arithmetic mean in place of the geometric mean when either value was less than one-tenth of the other. This method was found to have superior convergence properties over methods using the arithmetic mean exclusively.

The position amplitude, peak rate, and period of the corresponding stable limit cycles are plotted against their corresponding gain parameters in Figs. 5, 6, and 7. The position amplitude of Fig. 5 approximates a $1.445\ \pi/K_2$ relationship. The dispersion in the data appears to be the result of errors in determining the precise zero crossings of the discrete time solution of the transient response. The peak limit cycle rate approximates $8.354/K_3$. In this case the apparent dispersion is presumed to be valid data since a correlation to the reciprocal of the position gain K_2 was also identified. The influence of the position and rate gains on the limit cycle period is readily apparent in the limit cycle period of Fig. 7. Taken together, Figs. 5, 6, and 7 indicate that simultaneous minimization of position amplitude and peak rate along with maximum period represent mutually exclusive constraints on the integral, position, and rate gains. However, this conflict may

be resolved by minimizing a mean square rate which can be approximated by the rate squared, divided by the period.

B. Application to the 70-m Axis Servos

The dynamics of the 70-m antenna axis servos are far more complicated than those of the elementary PID controller described above, but the same principles of analysis apply. A simplified dynamic block diagram of the typical axis rate servo is shown in Fig. 8 where a rigid body approximation of the actual antenna structure is assumed. To condense the state-space model to the minimum number of states, the lead network in the tachometer feedback path is replaced with the equivalent acceleration-state feedback in Fig. 9 and the network pole at $-P_1$ is ignored. To accommodate representation by open-loop and closed-loop state-space matrices, the position loop controller of Fig. 8 is replaced in Fig. 9 by the equivalent feedback gains which operate on the multivariable output Y. This distinction between the output and the states will become apparent when the nonlinearities are introduced.

With the conventional state-space representation of the system,

$$\dot{x} = \mathbf{A}x + \mathbf{B}U$$

$$Y = \mathbf{C}x + \mathbf{D}U$$

The multivariable **A B C D** matrices, before incorporating the position loop control gain K, are

$$\mathbf{A} = \begin{bmatrix} 0 & 1 & 0 & 0 & 0 \\ 0 & 0 & 1 & 0 & 0 \\ 0 & 0 & 0 & 1/J_m & 0 \\ 0 & 0 & -(V^2 + K_R)/C_h & -(D_h + K_R/J_m Z_1)/C_h & (Z_2 - P_2)/C_h \\ 0 & 0 & -K_R & -K_R/J_m Z_1 & -P_2 \end{bmatrix}$$

$$\mathbf{B} = \begin{bmatrix} 0 & 0 & 0 \\ 1 & 0 & 0 \\ 0 & 1/J_m & 0 \\ K_R/C_h & -K_R/J_m Z_1 C_h & V/C_h \\ K_R & -K_R/J_m Z_1 & 0 \end{bmatrix}$$

$$\mathbf{C} = \begin{bmatrix} 1 & 0 & 0 & 0 & 0 \\ & 1 & 0 & 0 & 0 \\ & & 1 & 0 & 0 \\ & & & 1/J_m & 0 \end{bmatrix} \qquad \mathbf{D} = \begin{bmatrix} 0 & 0 & 0 \\ 0 & 0 & 0 \\ 0 & 0 & 0 \\ 0 & 1/J_m & 0 \end{bmatrix}$$

where the multivariable input U and output Y correspond to

$$U = \begin{bmatrix} -KY \\ \text{external torque} \\ \text{excess flow} \end{bmatrix} \qquad Y = \begin{bmatrix} \text{integral position} \\ \text{position} \\ \text{rate} \\ \text{acceleration} \end{bmatrix}$$

The excess flow element in the input vector U is included to accommodate the future addition of a nonlinear representation of the hydraulic valve.

Incorporating the controller gain K into the state equations involves some unusual complexity since U includes Y and Y is also dependent on U when the input matrix **D** is nonzero. The

fundamental state equations for $\dot{x}$ and Y can be expressed in a form to separate the $-KY$ from the other elements of U. Thus substituting $-\mathbf{B}_1 KY + \mathbf{B}U_{\text{Ext}}$ for $\mathbf{B}U$ and $-\mathbf{D}_1 KY + \mathbf{D}U_{\text{Ext}}$ for $\mathbf{D}U$ where $\mathbf{B}_1$ and $\mathbf{D}_1$ denote the first columns of $\mathbf{B}$ and $\mathbf{D}$ and U_{Ext} is U with the first element replaced by zero,

$$\dot{x} = \mathbf{A}x - \mathbf{B}_1 KY + \mathbf{B}U_{\text{Ext}}$$

$$Y = \mathbf{C}x - \mathbf{D}U = \mathbf{C}x - \mathbf{D}_1 KY + \mathbf{D}U_{\text{Ext}}$$

which leads to

$$Y = [I + \mathbf{D}_1 K]^{-1}(\mathbf{C}x + \mathbf{D}U_{\text{Ext}})$$

and

$$\dot{x} = \mathbf{A}x - \mathbf{B}_1 K[I + \mathbf{D}_1 K]^{-1}(\mathbf{C}x + \mathbf{D}U_{\text{Ext}}) + \mathbf{B}U_{\text{Ext}}$$

These expressions for Y and $\dot{x}$ define new $\mathbf{A}$ and $\mathbf{C}$ matrices for the general case involving position controller gain K.

In the specific case described here, the input U does not couple directly into Y since $\mathbf{D}_1$ is a column of zeros. Thus $\mathbf{C}$ is unaffected by introduction of the controller gain K and the expressions for the closed-loop $\mathbf{A}_1$ and $\mathbf{B}_1$ simplify to

$$\mathbf{A}_1 = \mathbf{A} - \mathbf{B}_1 K\mathbf{C}$$

$$\mathbf{B}_1 = \mathbf{B} - \mathbf{B}_1 K\mathbf{D}$$

The open-loop system matrices $\mathbf{A}_0$ and $\mathbf{B}_0$ are formed by altering the closed-loop $\mathbf{A}_1$ and $\mathbf{B}_1$ to satisfy the constraint that the rate state $\dot{x}_3$ and the acceleration output y_4 must remain zero. This is accomplished by assigning zeros to the third rows of $\mathbf{A}_0$ and $\mathbf{B}_0$, to the second column of $\mathbf{B}$, and to elements $a0_{4,3}$, $a0_{5,3}$, and $a0_{5,4}$ of $\mathbf{A}_0$ and changing $a0_{4,4}$ to $-\mathbf{D}_h/C_h$. This process is the equivalent of breaking the forward paths through $1/J_m$ and the (-1) and (-V) rate feedback paths. In actual practice, modifying the third columns of $\mathbf{A}$ and $\mathbf{C}$ is unnecessary because x_3 is already constrained to zero. For convenience in determining the breakaway condition, $\mathbf{C}$ and $\mathbf{D}$ are used unmodified in the open-loop case. This results in a finite value of the acceleration output y_4, which is tested for a zero crossing to determine the end of the open-loop condition.

As in the case of the elementary PID controller discussed earlier, the end points of the open-loop and closed-loop transients are determined by the zero crossings of the rate and of the control-friction torque difference. The determination of initial conditions is more complicated, however, because the governing physical friction law fails to uniquely define more than two of the five state variables. In the case of the closed-loop initial condition, the requirements of zero rate and acceleration define the third and fourth variables, whereas in the open-loop case the sole requirement of zero rate defines only the third variable. This difficulty was partially overcome by arbitrarily assigning a small value to the position variable and small time derivatives to the fourth and fifth state variables. Thus with x_2 and x_4 defined and $x_3 = 0$, x_1 and x_5 can be determined from solution of the matrix equation

$$\begin{bmatrix} a1_{4,1} & a1_{4,5} \\ a1_{5,1} & a1_{5,5} \end{bmatrix} \begin{bmatrix} x_1 \\ x_5 \end{bmatrix} + \begin{bmatrix} a1_{4,2} & a1_{4,4} \\ a1_{5,2} & a1_{5,4} \end{bmatrix} \begin{bmatrix} x_2 \\ x_4 \end{bmatrix} + \begin{bmatrix} b1_{4,1} & b1_{4,2} & b1_{4,3} \\ b1_{5,1} & b1_{5,2} & b1_{5,3} \end{bmatrix} \begin{bmatrix} 0 \\ T_{sf} \\ 0 \end{bmatrix} = \begin{bmatrix} \nu_4 \\ \nu_5 \end{bmatrix} \tag{2}$$

where T_{sf} represents the static friction and ν_4 and ν_5 represent the assigned values for $\dot{x}_4$ and $\dot{x}_5$ at time $t = 0+$. The use of the closed loop $\mathbf{A}_1$ and $\mathbf{B}_1$ in this expression ensures that the condition will be satisfied after the transient begins.

Figures 10, 11, and 12 illustrate the convergence resulting from the use of Eq. (2) for initial conditions with three different combinations of static and Coulomb friction. All three cases used initial conditions $x_2 = 0.02$ rad, $\nu_4 = -0.12$ rad/sec, and $\nu_5 = -0.01$ rad/sec. The plant variables are typical of the 70-m azimuth axis, and position control gain K is the phase-variable-form equivalent of the present values in the 70-m servo firmware [4]. Figures 10, 11, and 12 indicate that while the solutions always converge or diverge properly depending on the static–Coulomb friction difference, the initial conditions selected using Eq. (2) are far from those of the stable limit cycle.

Figure 11 indicates that unlike the elementary PID controller, the 70-m axis servos develops a finite limit cycle even when the levels of the static and Coulomb frictions are equal. A comparison of Figs. 10, 11, and 12 also seems to indicate a proportionality between the integral position amplitude and the static friction, as is the case for the elementary PID con-

troller. The magnitude of the proportionality constant is not obvious from the system equations.

IV. Conclusions

The piecewise linear method described here has been shown to be highly effective in evaluating friction-induced limit cycle behavior in the 70-m axis servos. The method is sufficiently general such that it should be readily applicable to treatment of hysteresis and deadzone effects in the hydraulic valve and other nonlinearities characterized by a discontinuity between linear properties. In the next stage of development it should be possible to identify the basic parametric relationships between the system parameters and limit cycle properties. A knowledge of these relationships will enable system designers to develop improved servo designs with less objectionable limit cycle properties.

References

[1] R. E. Hill, "A New State Space Model for the NASA/JPL 70-Meter Antenna Servo Controls," *TDA Progress Report 42-91*, vol. July-September 1987, Jet Propulsion Laboratory, Pasadena, California, pp. 285-294, November 15, 1987.

[2] R. E. Hill, "A New Algorithm Modeling Friction in Dynamic Mechanical Systems," *TDA Progress Report 42-95*, vol. July-September 1988, Jet Propulsion Laboratory, Pasadena, California, pp. 51-57, November 15, 1988.

[3] N. Minorsky, *Theory of Nonlinear Systems*, New York: McGraw-Hill, 1969.

[4] L. S. Alvarez and J. Nickerson, "Application of Optimal Control Theory to the Design of the NASA/JPL 70-M Antenna Axis Servos," *TDA Progress Report 42-97*, Jet Propulsion Laboratory, Pasadena, California, this issue.

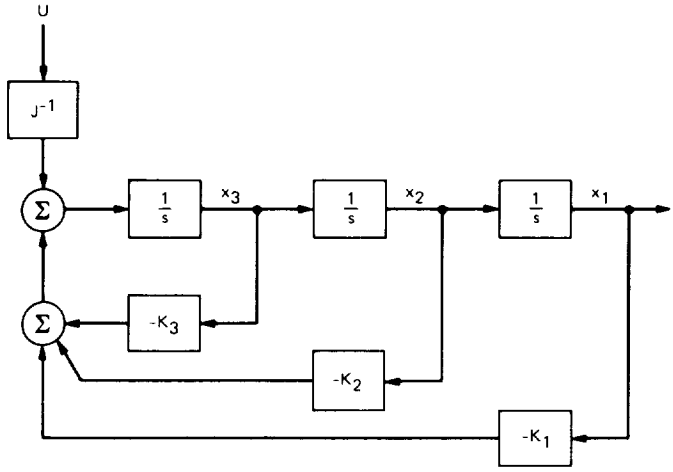

Fig. 1. Block diagram of an elementary PID controller.

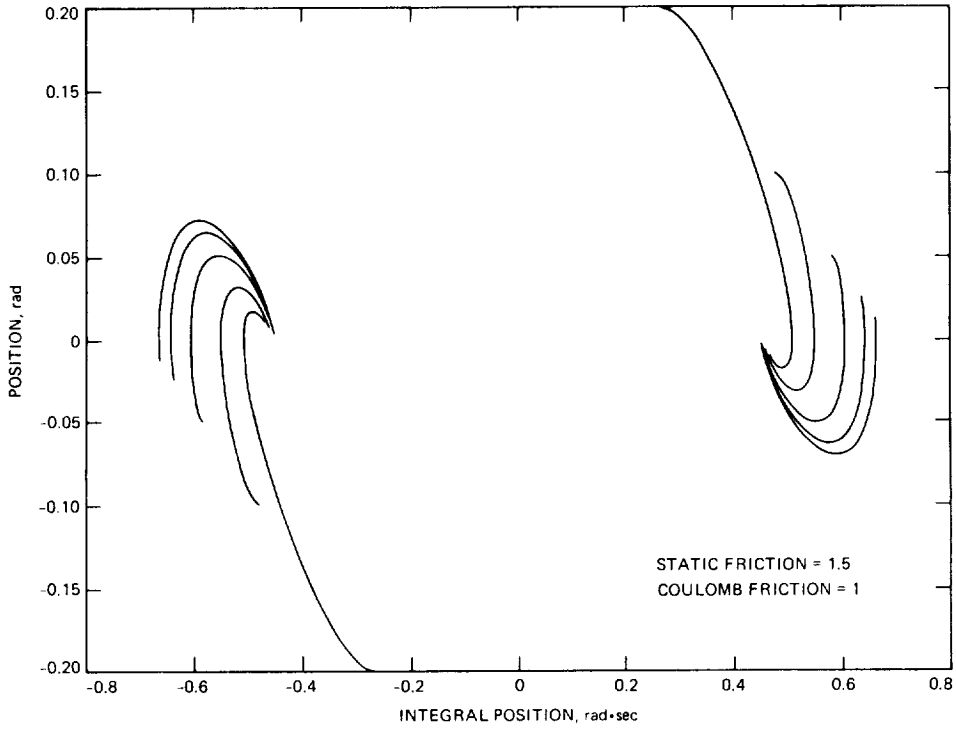

Fig. 2. Phase portrait of typical linear responses of the system in Fig. 1.

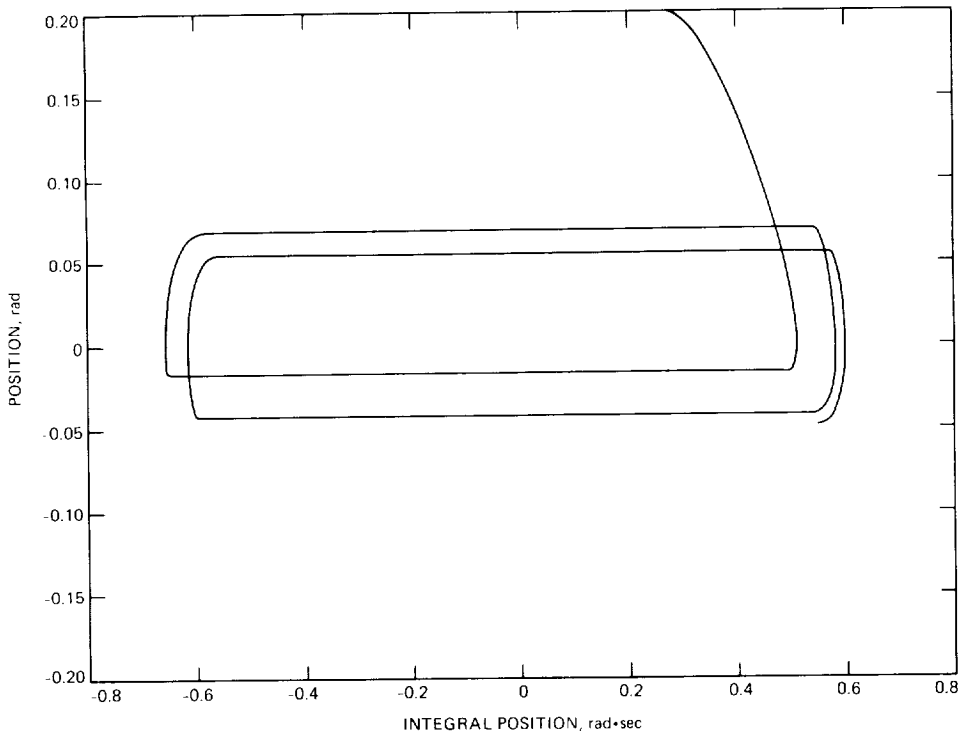

Fig. 3. Typical limit cycle portrait of the system in Fig. 1.

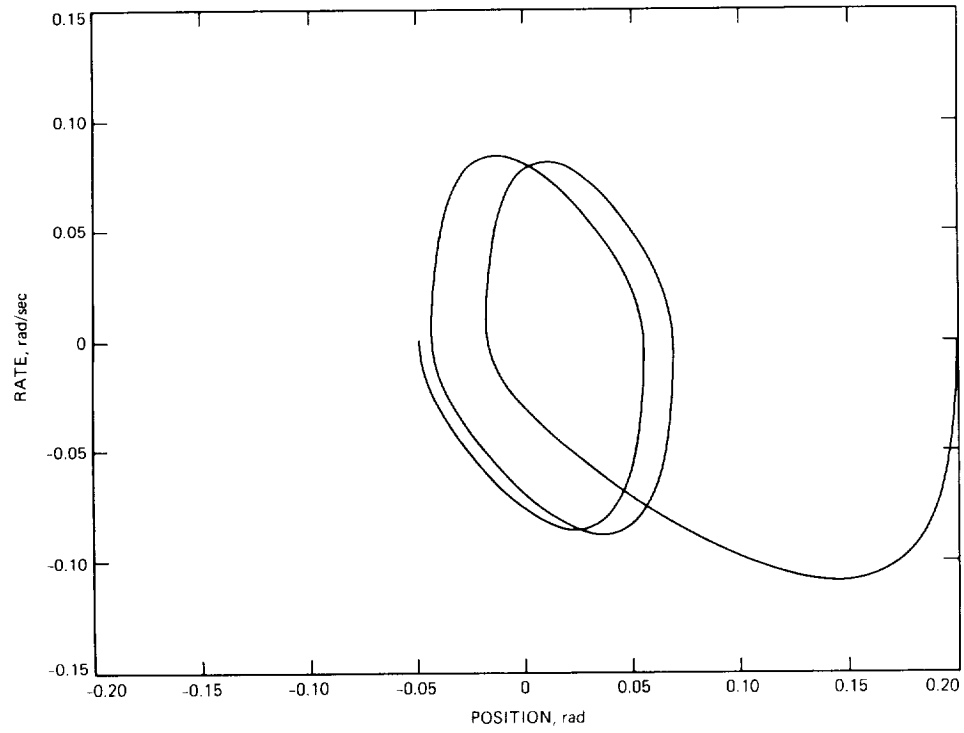

Fig. 4. Rate-plane projection corresponding to Fig. 3.

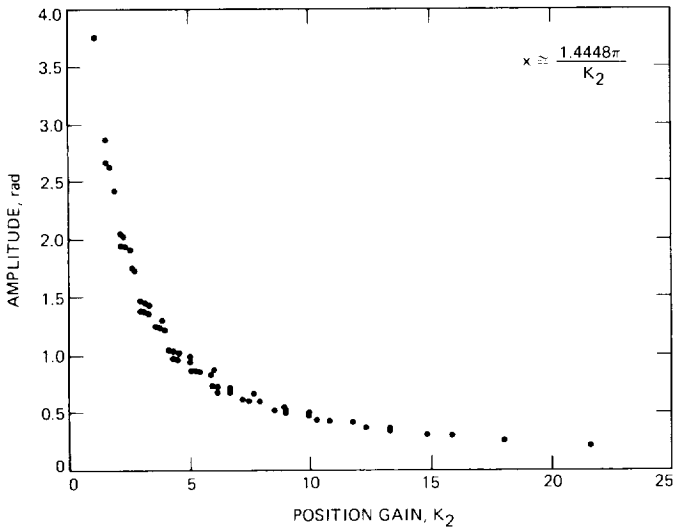

Fig. 5. Limit cycle position amplitude versus position gain for the system in Fig. 1.

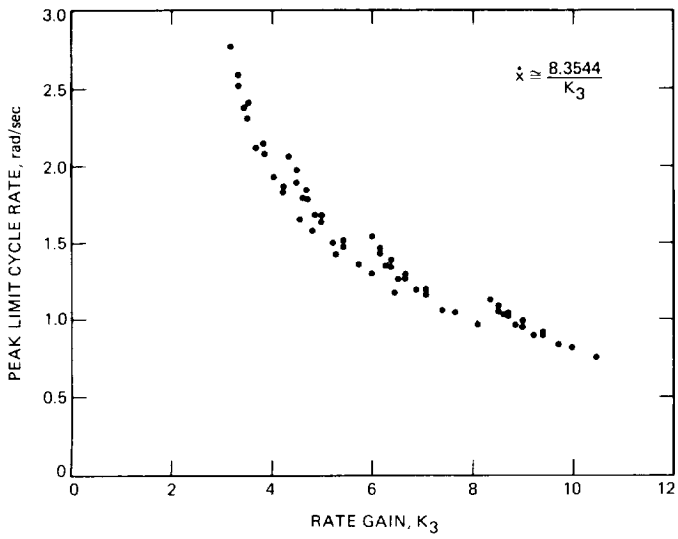

Fig. 6. Limit cycle peak-rate amplitude versus rate gain for the system in Fig. 1.

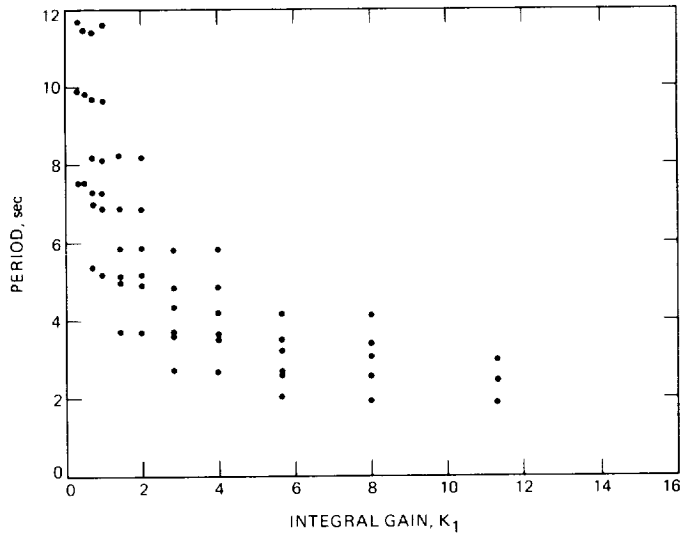

Fig. 7. Limit cycle period versus integral gain for the system in Fig. 1.

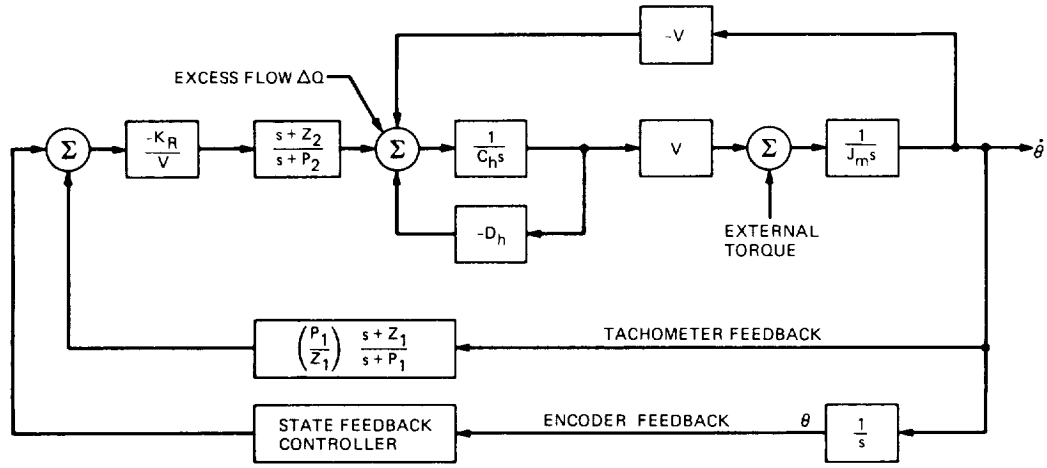

Fig. 8. Dynamic block diagram of the 70-m antenna axis servos.

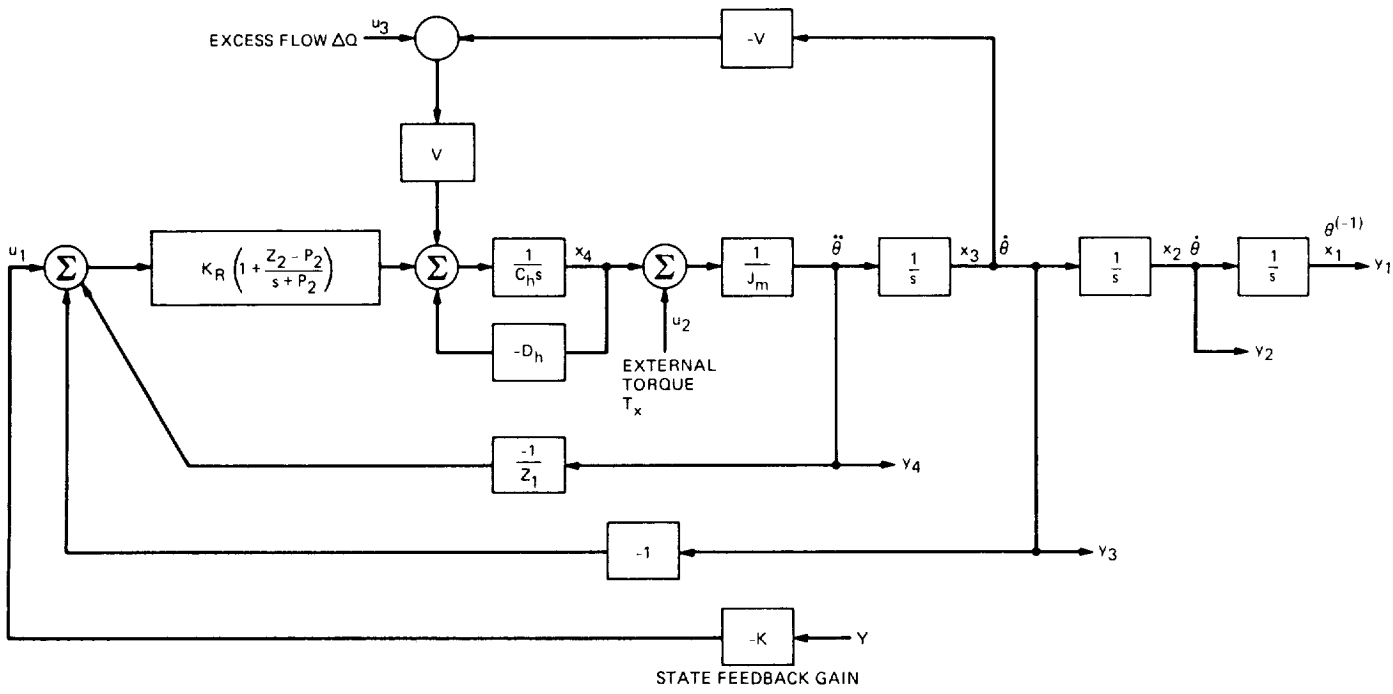

Fig. 9. Simplified multivariable system block diagram of the 70-m antenna axis servos.

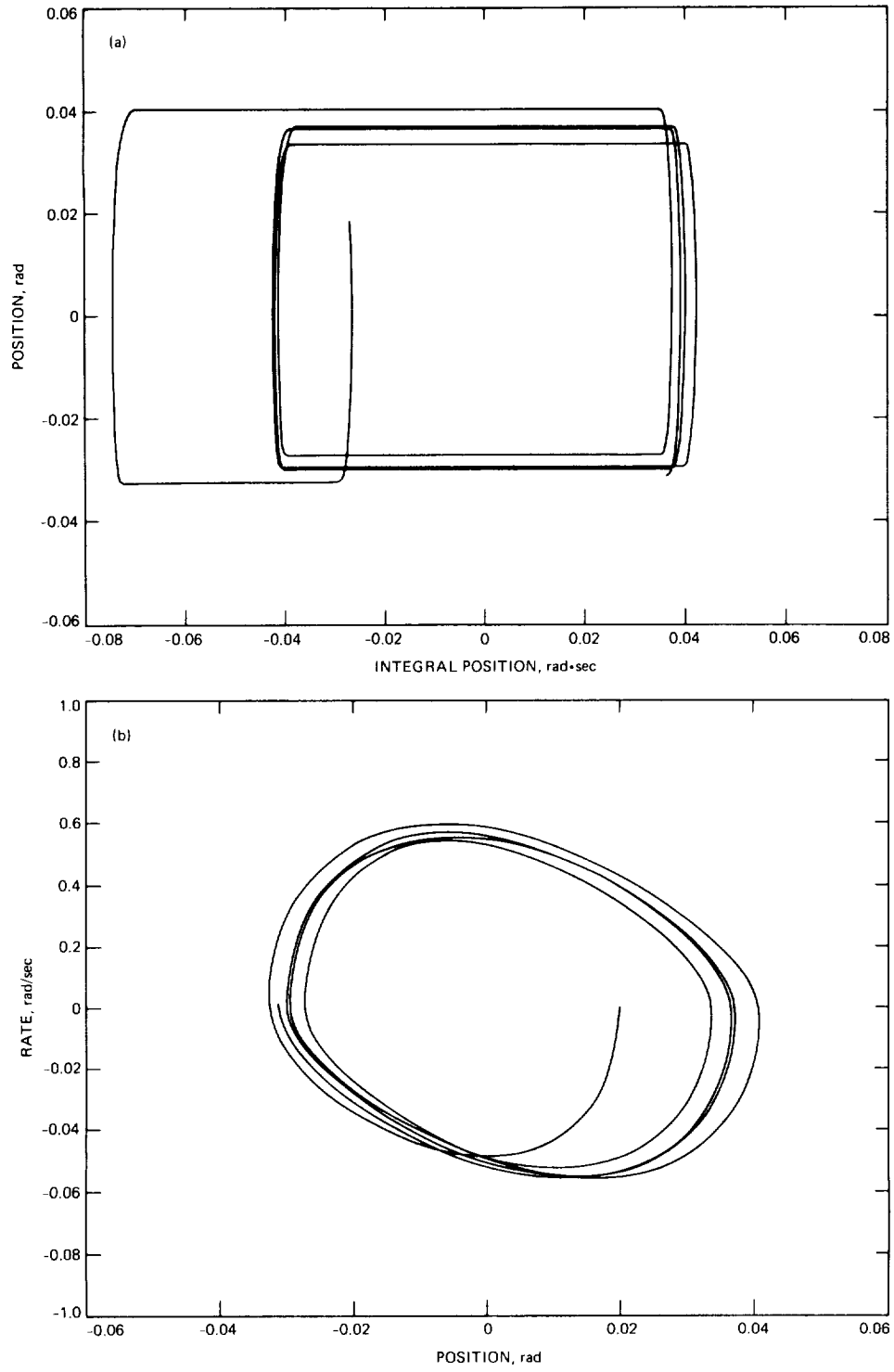

Fig. 10. 70-m axis servo limit cycle (T_{fs} = 500, T_{fc} = 250): (a) integral plane; (b) rate plane.

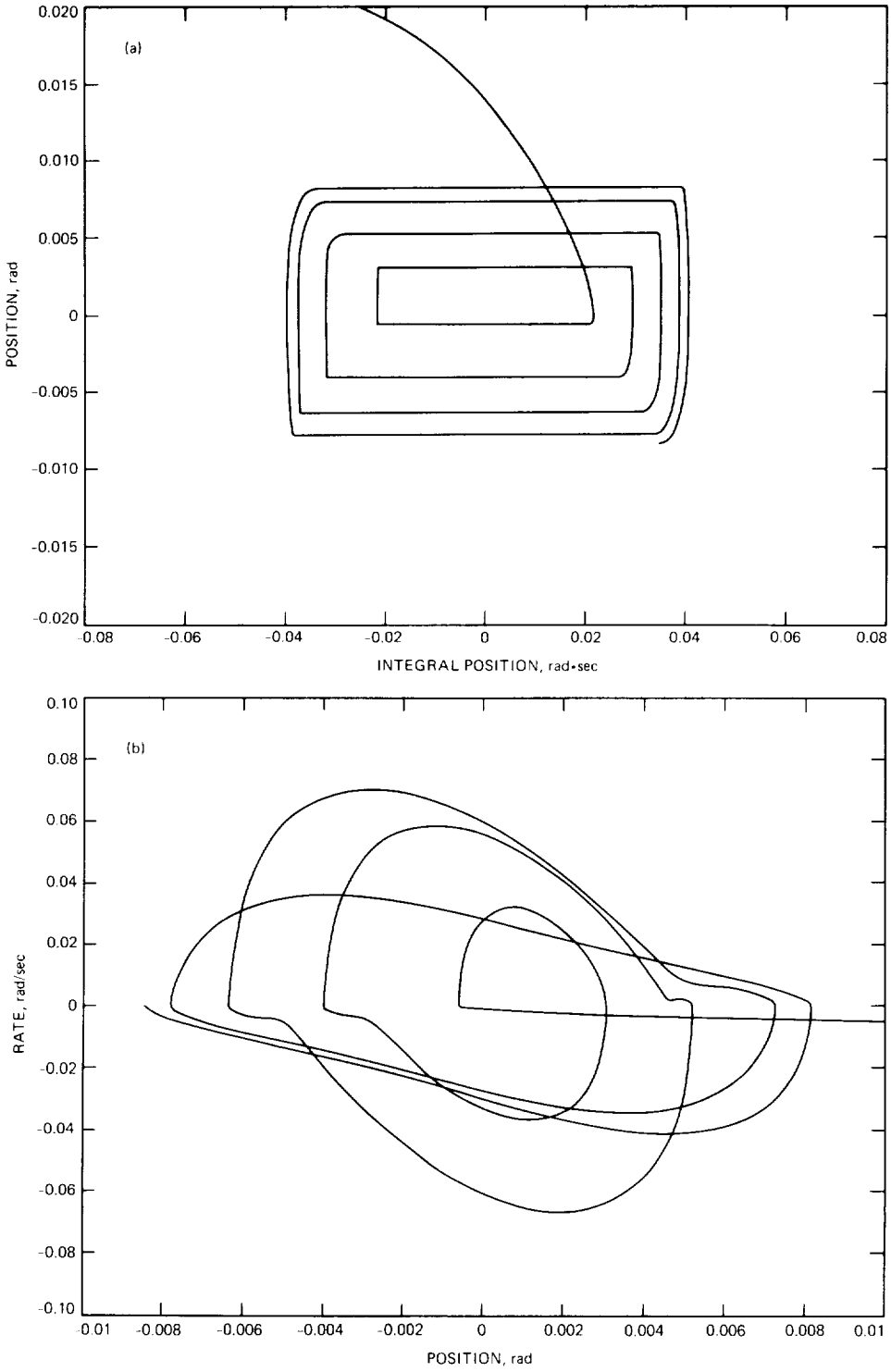

Fig. 11. 70-m axis servo limit cycle (T_{fs} = 500, T_{fc} = 500): (a) integral plane; (b) rate plane.

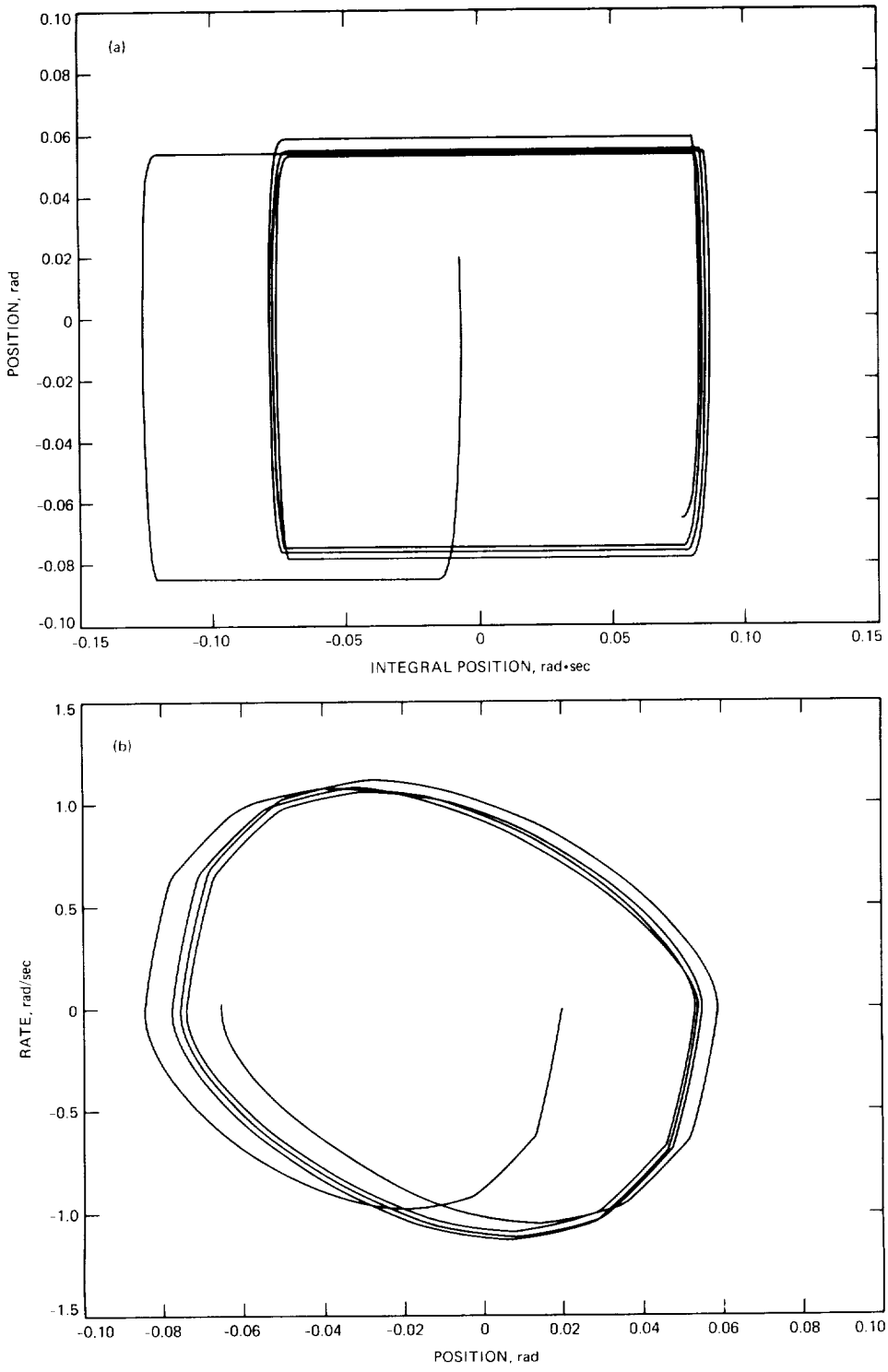

Fig. 12. 70-m axis servo limit cycle (T_{fs} = 1000, T_{fc} = 500): (a) integral plane; (b) rate plane.